Available online at www.sciencedirect.com

ScienceDirect

Energy Procedia 84 (2015) 93 – 98

Energy Procedia

E-MRS Spring Meeting 2015 Symposium C - Advanced inorganic materials and structures for photovoltaics

Characterization of a-Si:H solar cell modules on plastic substrates by high resolution LBIC technique

M. Fernandes[a,b]*, Y. Vygranenko[b], M. Vieira[a,b], A. Sazonov[c], R. Yang[c], A. Khosropour[c]

[a]*Electronics Telecommunications and Computer Engineering, ISEL, Lisbon, 1959-001, Portugal*
[b]*CTS-UNINOVA, Quinta da Torre, 2829-516, Caparica, Portugal*
[c]*Electrical and Computer Engineering, University of Waterloo, Waterloo, N2L 3G1, Canada*

Abstract

This article reports on characterization of hydrogenated amorphous silicon (a-Si:H) photovoltaic modules fabricated on 100 μm thick PEN plastic films. Experimental results show that the shunt leakage is one of the factors reducing the device performance. Current-voltage characteristics of individual a-Si:H p-i-n cells were analysed to estimate a variation of shunt resistances. A SPICE model of the a-Si:H p-i-n cell with local shunt leakage was also developed to analyse the impact of leakage currents on the device performance. Using the LBIC technique, the presence of multiple shunts in the cell was detected. They are attributed to surface defects in plastic foils, which are thermally induced during the device fabrication.

Peer-review under responsibility of The European Materials Research Society (E-MRS)

Keywords: amorhous silicon; thin-film solar cells; shunt leakage.

1. Introduction

Hydrogenated amorphous silicon (a-Si:H) solar cells on thin plastic substrates are recently gathering a great interest . Their true mechanical flexibility allows the integration with elements of various shapes and sizes enabling the fabrication of innovative solar products [1]. The radiation hardness of a-Si:H and high power-to-weight ratio of photovoltaic (PV) modules on thin plastic substrates, also make them suitable for extraterrestrial applications [2].

* Corresponding author. Tel.: +351-218 317 289; fax: +351-218 317 114.
E-mail address: mfernandes@deetc.isel.ipl.pt

Peer-review under responsibility of The European Materials Research Society (E-MRS)
doi:10.1016/j.egypro.2015.12.300

Regardless of the intense research efforts directed to the development of flexible a-Si:H solar cells on low-cost plastic substrates, these devices still exhibit considerably low performance in comparison to glass-based analogues. The major technological challenge is deposition of doped- and undoped a-Si:H layers with required electronic properties at temperatures lower than that for solar cells on glasses or metal foils [3]. The increased shunt leakage in a-Si:H cells on the plastic substrate is another challenging issue that we have observed in our PV modules [4]. Resistive shunts can significantly reduce the fill factor (FF) and the open circuit voltage (V_{oc}) thus decreasing the power conversion efficiency (PCE) [5]. Therefore it is necessary to understand the causes and mechanisms of electrical shunts in solar cells.

This paper reports on the shunt leakage in the a-Si:H solar cell array on plastic substrate and its impact on the device performance. Detailed description of the device design is the starting point of the presented work. The experimental section also describes high resolution Light Beam Induced Current (LBIC) technique used for shunts detection. Next, the current-voltage characteristics of individual cells are analyzed to estimate a variation of shunt resistances. The impact of leakage currents on device performance is analyzed through modelling. This follows with results on LBIC characterization. The nature of parasitic currents is also discussed analyzing the observed substrate defects. And finally, results of the study are summarized in the conclusion section.

2. Experimental

2.1. PV module design

The tested device is a monolithic 10 cm × 10 cm area PV module integrating an array of 72 a-Si:H n-i-p cells on a 100 µm thick polyethylene naphtalate (PEN) substrate. The cell design and its interconnections are illustrated in Figs. 1a and 1b. To relieve the mechanical strain, the backside encapsulation and front buffer a-SiO_xN_y layers are oxygen-rich and nitrogen-rich, respectively. Each cell is an a-Si:H *n-i-p* structure with Al/Cr and ZnO:Al layers serving as back and top electrodes, respectively. The photosensitive area of each cell is 1 × 0.8 cm^2. The sheet resistance of the 180-nm-thick ZnO:Al layer is about 60 Ω/sq. Two 0.3 mm wide Al fingers are symmetrically placed on the ZnO:Al electrode surface to reduce the emitter resistance. In the developed fabrication process, three shadow masks are used in sputtering steps to form the bottom and top electrodes, and top contacts. The *n-i-p* stack is deposited using a multi-chamber 13.56 MHz PECVD system at 150 °C. The deposition conditions for a-Si:H n-i-layers and a-SiC:H *p*-layer are reported elsewhere [6,7].

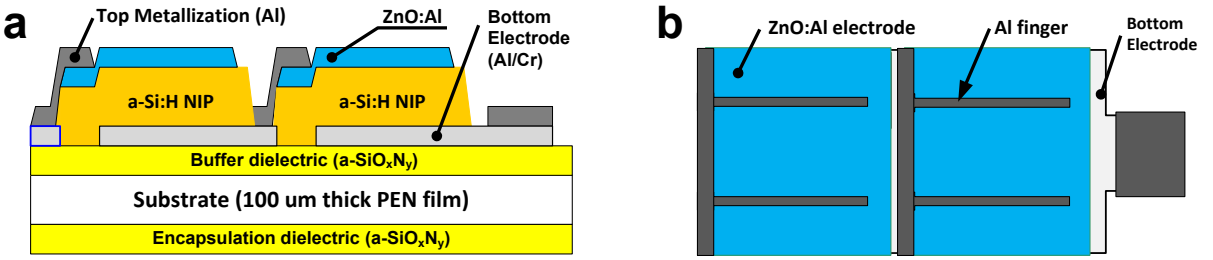

Fig. 1. Two cells connected in series: (a) cross-sectional view; (b) top view.

2.2. LBIC technique

Figure 2 shows a block-diagram of the developed LBIC system. The optical part of setup comprises a semiconductor red laser powered up by a pulse generator, a diaphragm limiting the beam diameter, a two-axis galvanometer scanner, and an F-Theta lens enabling a minimum light spot size of 16 um. The surface of the device is scanned by the modulated low-power laser beam and the induced current detected by a SR830 DSP lock-in amplifier. During the measurement procedure, the computer controls the scanner through DACs of the lock-in unit,

and synchronously reads out, processes and stores the data. The customized computer software was developed using .NET technology. MATLAB was also used to visualize the LBIC data.

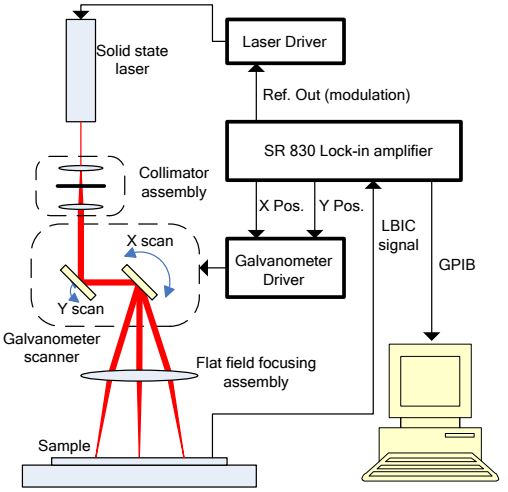

Fig. 2. LBIC measurement setup.

3. Results and discussion

The current-voltage (I-V) characterization of *n-i-p* cells in the module was performed using a Keithley 2400 measurement unit controlled by a PC with dedicated software. Fig. 3a shows comparison of dark I-V curves for cells with various magnitudes of the shunt leakage current. The measured current (I_{meas}) can be represented as a sum of two current components

$$I_{meas} = I_{diode} + I_{shunt}, \quad (1)$$

where I_{diode} is the diode current, and I_{shunt} is the shunt leakage current. For our device, I_{shunt} varies linearly with biasing voltage, what can be represented as a shunt resistance (R_{sh}). All 72 cells in the module were tested. The statistics on shunt resistances is shown in Fig. 3b, where the number of cells with certain ranges of shunt resistance in the module is shown in terms of its probability. The shunt resistance varies in the range from 10 to 10^5 Ω.

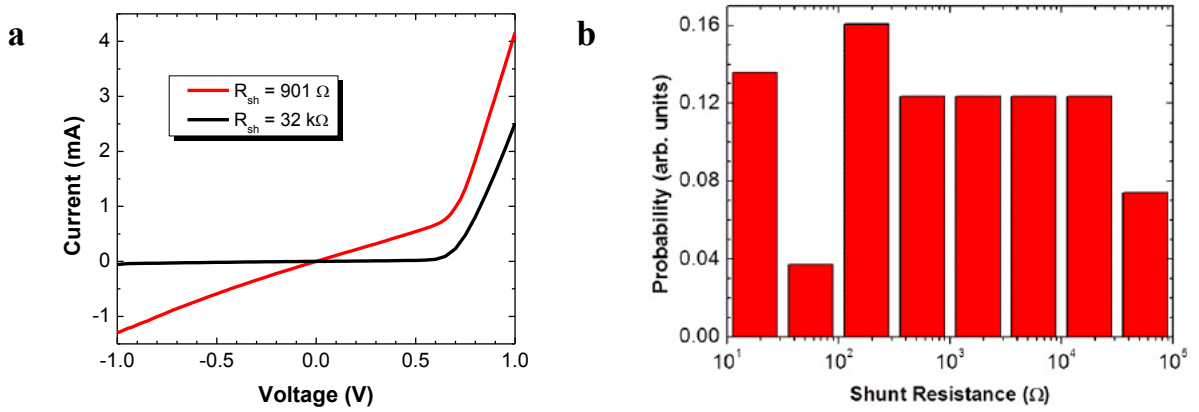

Fig. 3. (a) Current-voltage characteristics of a-Si:H n-i-p cells with low- and high shunt leakage; (b) Probability histogram showing distribution of cells with various shunt resistances in a module .

To estimate the effect of shunt leakage on output characteristics, we have performed device modelling using a two-dimensional distributed circuit model of the photovoltaic cell with a front metal grid [8]. The simulated cell is divided into equidimensional rectangular sub-cells with dimensions L_x and L_y. The equivalent circuit of the sub-cell is shown in Fig. 4a. It includes resistors R_x and R_y representing the top electrode, a resistor R_p, representing the resistance of the *p*-layer and contact resistance of the p/TCO interface, R_c, a diode, and a current source representing current generation in the *n-i-p* structure [8]. The sub-cell with a micro-shunt also includes a resistor R_{ms}. A single shunt in the middle of the cell is considered here for simplicity presentation. The following model parameters were used: the TCO layer sheet resistance, R_{TCO} = 60 Ω/sq., the top metal layer sheet resistance, R_{metal} = 0.2 Ω/sq., the contact resistance, R_c = 1.5 Ω·cm^2, the diode ideality factor, n = 1.5, the saturation current density, $J_o = 10^{-12}$ A/cm^2, and the short circuit current of 11 mA /cm^2.

The lateral current flow in the TCO and top metal layers is shown in Fig. 4b. The current density at node (i,j) is given by

$$J_{i,j} = \sqrt{\frac{(I_{x1} + I_{x2})^2}{4L_y^2} + \frac{(I_{y1} + I_{y2})^2}{4L_x^2}}, \tag{2}$$

where I_{x1}, I_{x2}, I_{y1}, I_{y2} are the X-Y plane current components associated with resistors R_{x1}, R_{x2}, R_{y1}, R_{y2}, respectively.

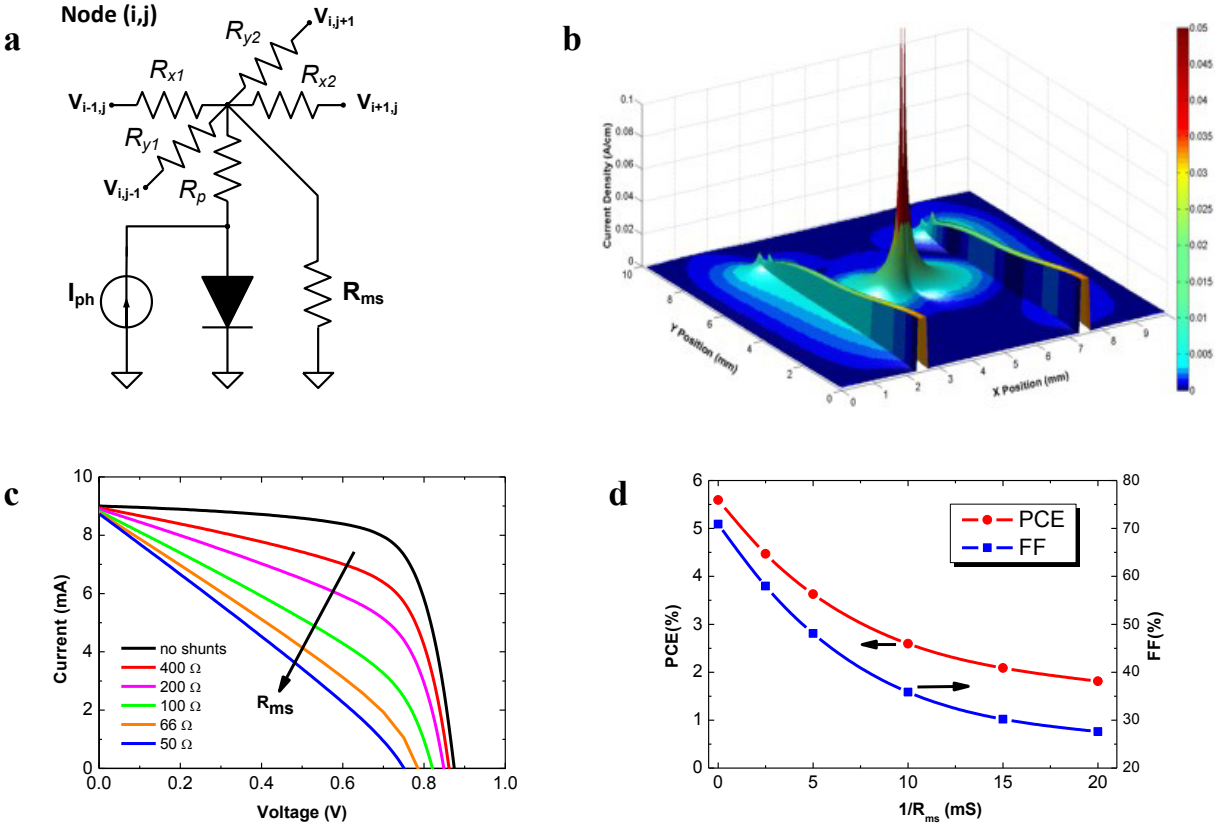

Fig. 4. SPICE modelling of the solar cell with a single shunt defect: (a) Equivalent circuit of the sub-cell with a micro-shunt; (b) Current density in the plane of the top contact; (c) Current-voltage characteristics at various micro-shunt resistances; (d) Power conversion efficiency and fill-factor as a function of the shunt conductance.

Note that in the sub-cell with the shunt, the I_{x1}, I_{x2} as well as I_{y1}, I_{y2} have opposite signs resulting in significantly lower current density in comparison to surrounding cells. That is why the current density peak in Fig.4b is split.

Figure 4c shows a comparison of current-voltage characteristics calculated at various micro-shunt resistances. The power conversion efficiency (PCE) and fill-factor as a function of the micro-shunt conductance are shown in Fig. 4d. Results show that at R_{ms} below 1 kΩ the fill-factor significantly decreases leading to PCE drop. Note that the R_{ms} representing a shunting microdefect and the R_{sh} denoting a general solar cell parallel resistance are not the same due to resistances of TCO and metallization layers.

The performed LBIC experiments show the presence of multiple shunts. The characterization was performed in dark and unbiased conditions to reduce the noise and to avoid artificial signal variations [9]. The ac component of the output voltage was measured when the device impedance was low (< 1 kΩ). Figure 5a shows a LBIC signal map indicating the shunt position manifested as decreased LBIC signal. In the absence of shunts the signal is constant over the whole area, excluding the metal finger area due to light blockage. Using the developed SPICE model, the LBIC signal was also simulated considering a single shunt at different locations. The laser beam induced photocurrent was simulated by sequential on/off switching of current sources in the sub-cell row containing the shunt (see Fig. 4a). Simulations where performed with shunts in different cell positions, for R_{ms} =100 Ω, and in the center of the cell for 50 Ω. Figure 5b shows the X-direction scan curves calculated at I_{ph} = 1 μA keeping the other model parameters as reported above. Modelling shows that the shunting microdefect affects the LBIC signal from an area much larger than its actual size since current from the surrounding area is shunted through the defect. In the case of single shunt, the signal minimum is a voltage drop across the resistor R_{ms}. The magnitude of signal variation depends on the sheet resistance of the TCO layer [10]. In the area shielded by the metal finger, the LBIC signal is almost constant that is in good agreement with the experimental LBIC results.

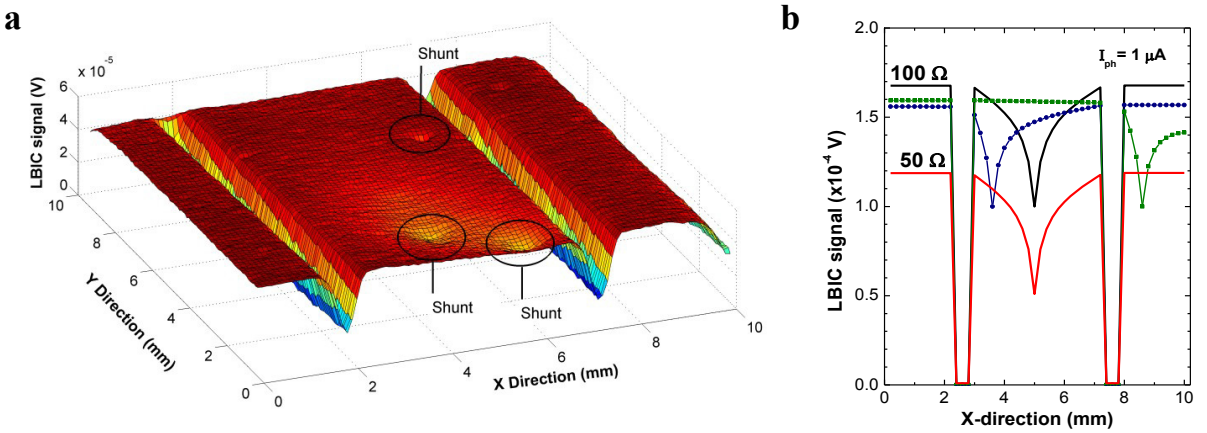

Fig. 5. (a) LBIC signal for cell with multiple shunts; (b) Calculated LBIC signals for 50 and 100 Ω shunts.

To understand the nature of electrical shunts, we analyzed the change in the surface roughness of all layers comprising individual solar cells throughout fabrication process. Fig. 6a shows an AFM surface scan of the a-Si:H layer revealing random surface peaks with height up to 150 nm. Micrograph of the top electrode in Fig. 6b also shows the presence of small dots. The density of these defects is much higher than what is expected from external contamination. Multiple experiments have confirmed that the defects appear after deposition of dielectric or semiconductor layers, or even after sputtering of metal layers on the PEN substrate. The reason is that cyclic oligomers, which are present in PEN, can migrate to the surface forming crystals, if the film is held at temperatures >100°C for tens of minutes [11]. The observed substrate defects may form microscopic pinholes, which are filled with highly conductive top layer material at the final process step, resulting in ohmic shunts.

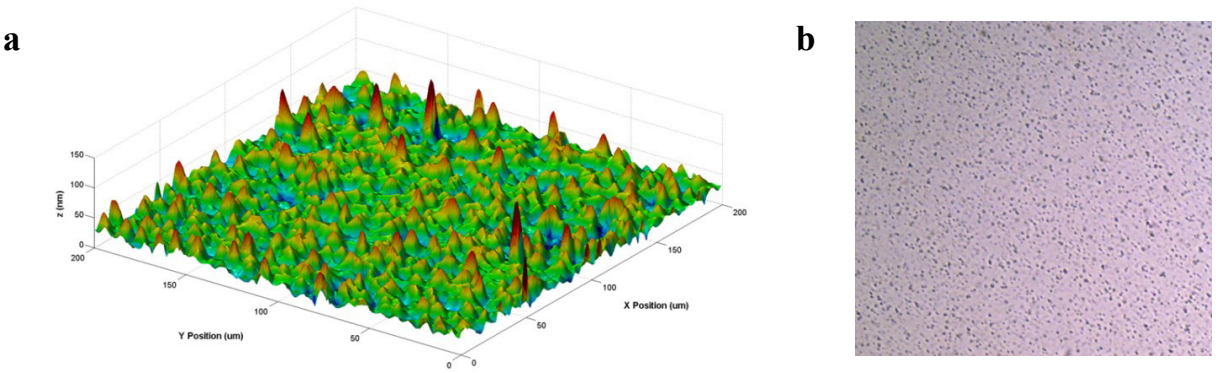

Fig. 6. (a) Surface scan of the a-Si:H film on the polyethylene-naphtalate (PEN) substrate; (b) Micrograph of top ZnO:Al layer.

4. Conclusion

We have performed analysis of electrical shunts in the a-Si:H PV module on PEN substrate. Current-voltage characterization of individual *n-i-p* cells shows that the shunt resistance varies in wide range from 10 to 10^5 Ω. SPICE modelling of the cell with a shunt defect has demonstrated the effect of shunt leakage on the output characteristics. Using the LBIC technique, multiple shunt defects were detected. Observed changes in surfaces roughness before and after deposition of layers suggests that shunts may be caused by thermally induced surface defects in plastic foils.

Acknowledgements

The authors are grateful to the Portuguese Foundation of Science and Technology through fellowship SFRH/BPD/102217/2014 and to Natural Science and Engineering Research Council (NSERC) of Canada for financial support of this research.

References

[1] M.B. Schubert and R. Merz. Flexible solar cells and modules. Philosophical Magazine 2009; 89: 2623-44.
[2] K. Beernink, S. Guha, et al. Lightweight, flexible solar cells on stainless steel foil and polymer for space and stratospheric applications. NASA/CP 2007; 214494 : 54-66.
[3] J.K. Rath, M.Brinza, Y.Liu, A.Borreman, and R.E.I.Schropp. Fabrication of thin film silicon solar cells on plastic substrate by very high frequency PECVD. Sol. Energ. Mater. Sol. Cell. 2010; 94: 1534-41.
[4] Y. Vygranenko, A. Khosropour, R. Yang, A. Sazonov, A. Kosarev, A. Abramov, and E. Terukov. Lightweight amorphous silicon photovoltaic modules on flexible plastic substrate. Canadian Journal of Physics 2014; 92(7/8): 871-874.
[5] M. Fortes, E. Comesana, J.A. Rodriguez, P. Otero, A.J. Garcia-Loureiro. Impact of series and shunt resistances in amorphous silicon thin film solar cells. Solar Energy 2014; 100: 114-123.
[6] K. H. Kim, Y. Vygranenko, D. Striakhilev, M. Bedzyk, J.H. Chang, A. Nathan, T.C. Chuang, G. Heiler, and T. Tredwell. Performance of a Si:H n–i–p photodiodes on plastic substrate J. Non-Crystal. Solids 2008; 354: 2590-2593.
[7] Y. Vygranenko, A. Sazonov, M. Vieira, G. Heiler, T. Tredwell, A. Nathan. Optimization of the a-SiC p layer in a-Si:H-based n-i-p photodiodes. Mater. Res. Soc. Symp. Proc. 2010; 1245: A18-01.
[8] Y. Vygranenko, M. Fernandes, M. Vieira, A. Khosropour, and A. Sazonov. A distributed SPICE model for amorphous silicon solar cells. Energy Procedia 2014; 60: 96 – 101.
[9] K. Zaunbrecher, S. Johnston, and J. R. Sites. Analysis of thin-film inhomogeneities using electroluminescence and LBIC Measurements. Proceedings of the 39th IEEE Photovoltaic Specialists Conference (PVSC), 2013; 166-169.
[10] P. Vorasayan, T.R.Betts, R.Gottschalg. Spatially distributed model for the analysis of laser beam induced current (LBIC) measurements of thin film silicon solar modules. Sol. Energ. Mater. Sol. Cell. 2011; 95: 111–114
[11] MacDonald, M. K. Looney et al. Latest advances in substrates for flexible electronics. Journal of the SID 2007;15(12): 1075.